

Ultrafast entropy production in pump-probe experiments

Lorenzo Caprini,^{1,*} Hartmut Löwen,¹ and R. Matthias Geilhufe^{2,†}

¹*Institut für Theoretische Physik II: Weiche Materie,
Heinrich-Heine-Universität Düsseldorf, 40225 Düsseldorf, Germany.*

²*Department of Physics, Chalmers University of Technology, 412 96 Göteborg, Sweden*

(Dated: February 7, 2023)

The ultrafast control of materials has opened the possibility to investigate non-equilibrium states of matter with striking properties, provided the sample of interest can sustain the strong fields often required. Hence, understanding ultrafast thermodynamic processes within the material are key. While slow processes lead to quasi-static changes in equilibrium, we focus here on the opposite limit of extremely short time scales, where the system rapidly approaches a non-equilibrium regime. Thermodynamic processes under fast driving were considered before, e.g. in Ref. [1], but have never been brought into connection with controlled experiments. Here, we derive a mesoscopic model for the entropy production due to non-equilibrium phonons excited by a THz laser pulse. While entropy cannot be measured directly, we show that the spectral entropy production can be obtained from experimentally observable quantities, which we illustrate using time-resolved X-ray scattering data for SrTiO₃. Further, we compute the spectral entropy production as a function of frequency for SrTiO₃ and KTaO₃ for various temperatures. Finally, we predict that the power spectrum of the displacement-displacement correlation function exhibits a broad peak besides the eigenmode-resonance, which is associated with entropy production.

Entropy production has been introduced in the 19-th century to describe the amount of irreversibility in thermodynamic cycles. It is behind the formulation of the Clausius inequality and the second law of thermodynamics. More generally, it characterizes heat and mass transfer processes at the macroscopic scales [2], such as heat exchange, fluid flow, or mixing of chemical species. Furthermore, in terms of information-entropy, it plays a significant role in information theory [3].

Successively, entropy production has been linked to microscopic dynamics [4] to quantify the amount of irreversibility and dissipation at the atomistic (single-particle) level [5, 6]. In the framework of gases, soft materials, or living organisms, each microscopic particle evolves in the presence of stochastic forces. These forces are usually generated by internal mechanisms, e.g., metabolic processes, internal motors, or collisions due to solvent molecules. The stochastic nature of the dynamics allows us to characterize macroscopic observables as averages of fluctuating variables, by considering the probability of observing a path of the microscopic trajectory. This approach is at the basis of stochastic thermodynamics [4], which aims of building the thermodynamic laws in terms of fluctuating work, heat, and entropy which on average are consistent with macroscopic thermodynamics [7].

In ordered phases of matter, we argue that thermal fluctuations of, e.g., ionic positions, spins, or charge lead to stochastic forces on microscopic degrees of freedom. Entropy is produced in non-equilibrium regimes, by excitations of the material with an external drive. This is motivated by immense progress in ultrafast control and characterization of crystalline solids [8–20]. We put specific focus on light-induced phonon dynamics [21–32]. Here, selected phonon modes are excited by strong THz

laser pulses [33, 34]. Remarkably, the ionic dynamics can be resolved with high precision with time-resolved X-ray scattering present at coherent X-ray light sources [35–47]. We deduce that the information obtained from such a scattering experiment is sufficient to reproduce the spectral entropy production rate within the material, giving rise to information about the ultrafast entropy production process.

Characterizing materials in terms of thermal properties in the ultrafast regime has emerged as a powerful path [16]. Hence, developing stochastic thermodynamics properties generated at short time scales, e.g. entropy production, could open new perspectives for the comprehension of functional materials. In the following, we show that non-equilibrium crystals, driven by a laser pulse, are characterized by spectral entropy production. As illustrated in Fig. 1, we propose to measure entropy production from ionic displacements, e.g., obtained from time-resolved X-ray scattering experiments. Further, we show that the power spectrum of ionic displacement shows a close connection to the spectral entropy production. We compare our theory to experimental data for SrTiO₃ and support our approach by providing estimates for the soft modes of KTaO₃ and SrTiO₃.

ULTRAFAST STOCHASTIC THERMODYNAMICS OF CRYSTALS

We model the dynamics of an optical phonon mode by the equation of motion [48–56]

$$\ddot{u}(t) + \eta\dot{u}(t) + \omega_0^2 u(t) = \sqrt{2\eta k_B T} \xi(t) + F(t), \quad (1)$$

Here, k_B is the Boltzmann constant while $u(t)$ is a phonon normal mode (units $\text{\AA}\sqrt{\text{a.m.u}}$) with frequency

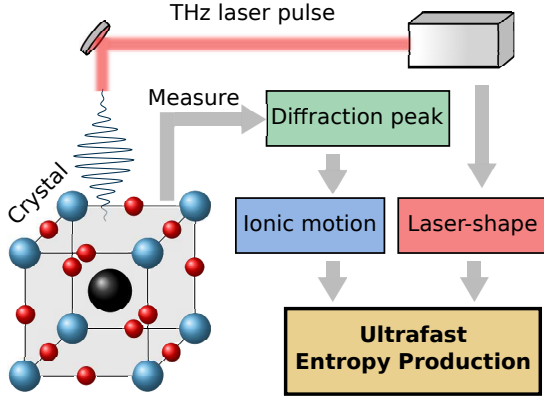


FIG. 1. Schematic representation of a crystal (SrTiO₃ or KTaO₃) excited by a THz laser pulse. From a direct measure of the diffraction pattern, for instance, obtained from time-resolved X-ray scattering experiments, the ionic displacement can be deduced. Combining this measure with the shape of the THz laser pulse, we can calculate the ultrafast entropy production by applying our theoretical results.

ω_0 , and damping or line width η . $F(t)$ is an external driving field, which, for a laser excitation can be written as $F(t) = Z\tilde{E}(t)$. Z is the mode effective charge [57], $\tilde{E}(t) = \epsilon^{-1}E(t)$ the screened electric field, and ϵ the relative permittivity.

For simplicity, we neglect nonlinear effects [23, 55, 56, 58]. In contrast to previous work, we add an uncorrelated noise $\sqrt{2\eta k_B T} \xi(t)$ modelling the interaction of the phonon normal mode with thermally excited lattice fluctuations ξ with the temperature of the environment T . The equation of motion (1) has a formal solution in Fourier space, given by

$$\hat{u}(\omega) = \chi(\omega) \left(\sqrt{2\eta k_B T} \hat{\xi}(\omega) + \hat{F}(\omega) \right), \quad (2)$$

with the susceptibility $\chi(\omega) = (\omega_0^2 - \omega^2 + i\eta\omega)^{-1}$. An example of the solution in real-time is reported in the appendix. Let $u = \{u\}$ denote a specific solution or trajectory between the initial time t_0 and the final time \mathcal{T} , with the initial conditions u_0 . The presence of thermal noise in the equation of motion introduces a final probability of realizing $\{u\}$, given by $P[\{u\}|u_0]$. The force $F(t)$ breaks the time-reversal symmetry. As a consequence, the probability of observing the time-reversed path $P_r[\{u\}|u_0]$ differs from $P[\{u\}|u_0]$ [59–61]. This leads to entropy production, Σ ,

$$\Sigma = k_B \log \frac{P[\{u\}|u_0]}{P_r[\{u\}|u_0]} = \int dt \sigma(t). \quad (3)$$

where $\sigma(t)$ is the entropy production rate. In the case of uncorrelated noise $\langle \xi(t)\xi(t') \rangle \sim \delta(t-t')$, the entropy production rate (Eq. (3)) is given by $\sigma(t) = \langle v(t)F(t) \rangle / T$, with $v(t) = \dot{u}(t)$ [4, 60]. Note, that this relation is general and thus also holds for non-linear phonon dynamics.

By decomposing Σ in Fourier waves, we introduce the spectral entropy production $\hat{\sigma}(\omega)$ as

$$\hat{\sigma}(\omega) = \int d\omega' S_r(\omega, \omega'), \quad (4)$$

with the entropy spectral density

$$S_r(\omega, \omega') = \frac{i}{T} \omega' \chi(\omega') \hat{F}(\omega') \hat{F}(\omega - \omega'). \quad (5)$$

Equations (4) and (5) are central theoretical results of the paper. With the knowledge of the susceptibility and the shape of the applied drive, quantities typically accessible in experiments, the spectral entropy production can be determined (Fig. 1). As a result, our predictions hold beyond phonons and can be applied for other excitations. In stochastic systems, the entropy production rate is a real fluctuating observable but its time average is positive in agreement with the second law of thermodynamics. In contrast, spectral entropy production is generally complex. To shed light on the interpretation of the spectral entropy production $\hat{\sigma}(\omega)$, we note it can be evaluated analytically for a periodic driving field $F(t) = A \exp(i\omega_d t)$. The imaginary part of the entropy production follows to be $\Im \hat{\sigma} = \delta(\omega - 2\omega_d) A^2 (T)^{-1} \omega_d (\omega_0^2 - \omega_d^2) ((\omega_0^2 - \omega_d^2)^2 + \eta^2 \omega_d^2)^{-1}$. Hence, it shows a delta peak at twice the driving frequency ω_d . Furthermore, it is negative (positive) if the driving frequency ω_d is larger (smaller) than the eigenfrequency ω_0 . In contrast, the real part $\Re \hat{\sigma} = \delta(\omega - 2\omega_d) A^2 (T)^{-1} \omega_d^2 \eta ((\omega_0^2 - \omega_d^2)^2 + \eta^2 \omega_d^2)^{-1}$ is an odd function of the damping η . Therefore, $\Re \hat{\sigma}$ vanishes for zero damping. Hence, $\Re \hat{\sigma}$ is a measure of dissipation associated with η . Both, $\Im \hat{\sigma}$ and $\Re \hat{\sigma}$ decrease with the distance between eigenfrequency ω_0 and driving frequency ω_d as well as with increasing temperature.

THE POWER SPECTRUM AND SPECTRAL ENTROPY PRODUCTION

The spectral entropy production can be determined from the frequency profile of the external force, e.g. THz laser pulses, and the susceptibility of the system. Alternatively, the power spectrum $\langle u(t)^2 \rangle$ can be expressed in terms of the entropy production generated by the laser excitation and, therefore, can be used to extract ultrafast thermodynamics properties of the system. Evaluating $\langle u(t)^2 \rangle$ in Fourier space, the power spectrum can be decomposed in two contributions as (see detail in the appendix)

$$\mathcal{F}[\langle u(t)^2 \rangle](\omega) = \mathcal{F}[\langle u(t)^2 \rangle]_{\text{eq}}(\omega) + \mathcal{F}[\langle u(t)^2 \rangle]_{\text{neq}}(\omega). \quad (6)$$

The first one $\mathcal{F}[\langle u(t)^2 \rangle]_{\text{eq}}$ has an equilibrium origin and, indeed, arises from thermal fluctuations,

$$\mathcal{F}[\langle u(t)^2 \rangle]_{\text{eq}} = 2\eta k_B T \delta(\omega) \int \frac{d\omega'}{2\pi} \hat{\chi}(\omega') \hat{\chi}(-\omega'). \quad (7)$$

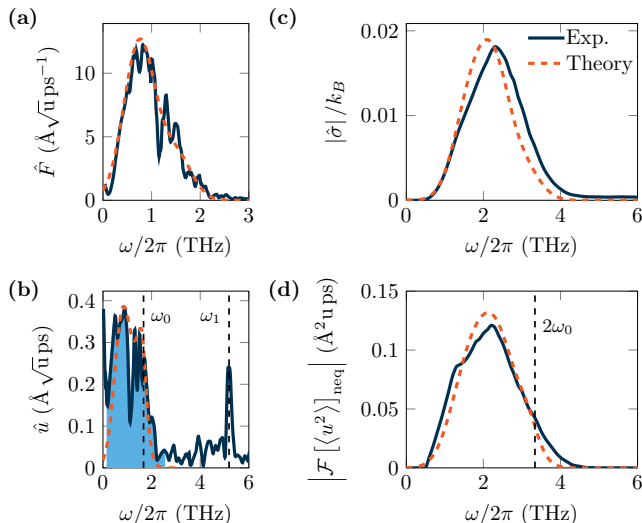


FIG. 2. Entropy production in SrTiO₃ after exposure to an intense THz laser pulse at 100 K. We compare an estimate computed from time-resolved X-ray scattering data taken from Kozima *et al.* [23] with model data. (a) Fourier transform of the THz laser pulse (solid dark blue), compared with a theoretical Gaussian laser pulse (orange dashed) with frequency $\omega_d = 0.75$ THz, superposed with a higher-harmonic at $2\omega_d$. (b) Comparison of experimental (solid dark blue) and computed (dashed orange) Fourier transform of the phonon normal mode amplitude, $\hat{u}(\omega)$. The soft mode contribution is shaded in light blue. (c) Comparison of the spectral entropy production, $|\hat{\sigma}|$, computed from the full experimental data of the phonon normal mode amplitude (solid dark blue) with our model taking into account the soft mode only (dashed orange). (d) Comparison of the power spectrum, $|\mathcal{F}[\langle u^2 \rangle]_{\text{neq}}|$, computed from the full experimental data (solid dark blue) with our soft-mode-only model (dashed orange).

As a result, it is $\propto T\delta(\omega)$ and fully determined by the susceptibility χ .

In contrast, the term $\mathcal{F}[\langle u(t)^2 \rangle]_{\text{neq}}$ originates from the external field (THz laser pulse) and, thus, reflects the non-equilibrium part of the dynamics. Indeed, this term (see appendix) can be expressed in terms of the entropy spectral density, $S_r(\omega, \omega')$, and reads

$$\mathcal{F}_\omega \langle u^2(t) \rangle_{\text{neq}} = T \int \frac{d\omega'}{2\pi} \frac{\hat{\chi}(\omega - \omega')}{(i\omega')} \hat{S}_r(\omega, \omega'). \quad (8)$$

Relation (8) is a key result of the paper providing an alternative route to measure the spectral entropy production. It shows that the ultrafast spectral entropy production in crystals can be measured from the power spectrum of the phonon displacement, an observable signature.

APPLICATION TO SrTiO₃ AND KTaO₃ UNDER LASER PULSES

To show that the entropy production rate can be obtained from experiments, we compare our model to time-

resolved X-ray scattering data obtained by Kozima *et al.*, for the nonlinear excitation of phonons in SrTiO₃ [23]. The spectral components of the used THz laser pulse are shown in Fig. 2 (a). To sufficiently reproduce the shape of the spectrum, we assume a superposition of two Gaussian laser pulses, one at frequency $\omega_d = 0.75$ THz and a higher-harmonic component with $2\omega_d$, $F(t) = Z\tilde{E}_0 (\exp(2\pi i\omega_d t) + \alpha \exp(4\pi i\omega_d t)) \exp(-\frac{1}{2} \frac{t^2}{\tau^2})$, with $\alpha \approx 0.2858$. The in-medium field strength is βE_0 , with $\beta = 0.215$ and $E_0 = 480$ kV cm⁻¹, while the pulse width is $\tau = 0.5$ ps. The experiment was performed at 100 K, where the soft mode frequency is measured to be $\omega_0/2\pi \approx 1.669$ THz with a damping of $\eta/2\pi \approx 0.9$ THz. The mode effective charge of SrTiO₃ is $Z = 2.6 e^- u^{-1/2}$ [23, 62], with e^- the elementary charge and u the atomic mass unit.

The measured spectral component of the time-domain X-ray data [23] is scaled against the computed amplitude of the soft mode according to Eq. (2) and shown in Fig. 2 (b). The soft mode contribution to the experimental spectrum is shaded in light blue. Data are used to compute the spectral entropy production, $|\hat{\sigma}|$, of the soft mode as a function of ω and compared against our theory in Fig. 2 (c). $|\hat{\sigma}|$ computed from the experimental data exhibits a peak at frequency $\omega_{\sigma_1}/2\pi \approx 2.33$ THz, that is reproduced by our model. Furthermore, we reconstruct the power spectrum, $|\mathcal{F}[\langle u^2 \rangle]_{\text{neq}}|$, given in Fig. 2 (d), which is off-resonance with twice the soft-mode frequency. The shape of $|\mathcal{F}[\langle u^2 \rangle]_{\text{neq}}|$ shows strong overlap with the computed entropy production. Due to nonlinear coupling between phonons, discussed in Ref. [23], a peak of the second optical mode at ≈ 5.19 THz can be clearly observed in Fig. 2 (b). We note that this mode (not considered in our model) is silent because there is no spectral overlap with the driving field, which is almost zero for $\omega > 3$ THz. As a result, the entropy production generated by the second optical mode and the laser field is negligible (compare Fig. 2 (b) and Fig. 2 (c), see also appendix).

To shed light on the process of entropy production due to laser fields, we compute the spectral entropy production for two different materials SrTiO₃ and KTaO₃, upon assuming a simple Gaussian laser pulse, $F(t) \sim e^{2\pi i\omega_d t}$ without higher-harmonic contribution. We fix the in-medium field strength to be $\tilde{E}_0 = 100$ kV cm⁻¹. As before, the frequency of the driving field is $\omega_d = 0.75$ THz and the pulse width is $\tau = 1$ ps. The mode effective charges are, SrTiO₃: $Z = 2.5$ [23, 62], KTaO₃: $Z = 1.4$ [62, 63]. We focus on the soft mode only, where frequency and line width strongly depend on temperature [64, 65] (see appendix).

SrTiO₃ is a cubic perovskite with a tetragonal phase transition at ≈ 105 K [66]. Further, SrTiO₃ exhibits a diverging dielectric constant at low temperatures as well as an asymptotic vanishing of the soft-mode fre-

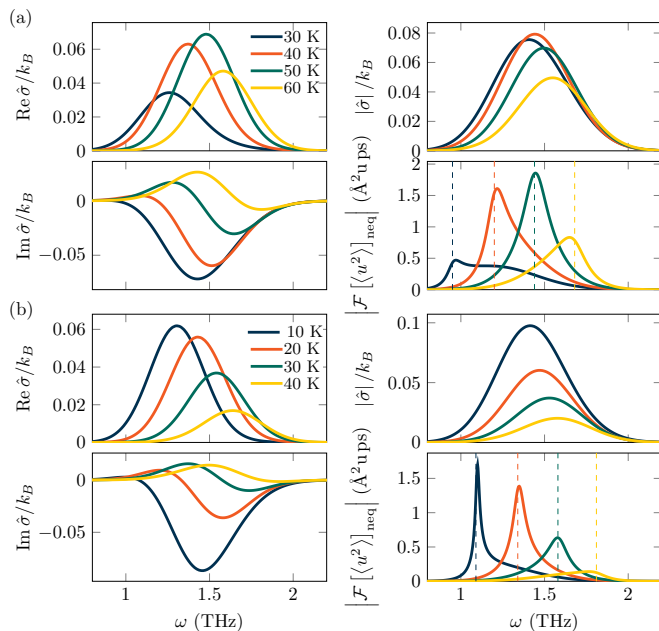


FIG. 3. Ultrafast thermodynamics properties for SrTiO₃ (a) and KTaO₃ (b). In each case, real part $\text{Re } \hat{\sigma}(\omega)$, imaginary part $\text{Im } \hat{\sigma}(\omega)$ and modulus $|\hat{\sigma}(\omega)|$ of the spectral entropy production, $\hat{\sigma}(\omega)$, (see definition (4)), are shown together with the Fourier transform of the non-equilibrium contribution of the power spectrum $\mathcal{F}_\omega \langle u^2(t) \rangle_{\text{neq}}$. Temperature-dependent soft modes are considered. Dashed lines in the plot for $\mathcal{F}_\omega \langle u^2 \rangle_{\text{neq}}$ denote twice the soft-mode frequency.

quency, both indicative of a ferroelectric phase transition [65, 67]. However, the transition is avoided due to quantum fluctuations, making SrTiO₃ a quantum critical paraelectric [67]. According to Ref. [64], the soft-mode frequency of SrTiO₃ is in resonance with the driving frequency, $\omega_0 = \omega_d = 0.75$ THz at $T \approx 52$ K. In Fig. 3 (a), we show the computed spectral entropy production for SrTiO₃ at various temperatures ranging from 30 K to 60 K. Due to the temperature dependence and softening of the damping, the real part becomes maximal slightly above 50 K. In contrast, the imaginary part of $\hat{\sigma}(\omega)$ increases with decreasing temperature, showing a clear sign change below 52 K. The absolute value of the spectral entropy production shows a local maximum around this temperature. However, as low temperatures suppress the thermal noise, entropy production by the non-equilibrium force is enhanced. As a result, the absolute value will increase rapidly for very low temperatures (<15 K, not shown here). Due to the narrow width of the Gaussian laser field (1 ps), neither $\text{Re } \hat{\sigma}$, $\text{Im } \hat{\sigma}$, nor $|\hat{\sigma}|$ have a peak at exactly $2\omega_d$, but instead show a decreasing peak frequency with decreasing temperature. Plotting $\mathcal{F}_\omega \langle u^2 \rangle_{\text{neq}}$ reveals clear peaks at twice the soft-mode frequency, which is indicated by dashed lines. A non-symmetric broadening of the peak for frequencies occurs in agreement with the spectral weight of the spectral en-

trophy production $\hat{\sigma}$. This becomes specifically apparent for the temperatures 30 K, 40 K and 60 K, in agreement with the notion of entropions [68].

In contrast to SrTiO₃, KTaO₃ remains cubic to liquid helium temperatures [69]. It is also regarded a quantum paraelectric, but outside the quantum critical regime [70]. As a result, the decrease of the soft-mode frequency and damping is slower compared to SrTiO₃, being in resonance with the driving frequency $\omega_d = 0.75$ THz at ≈ 26.4 K [64]. Therefore, we evaluate the spectral entropy production for temperatures between 10, ..., 40 K, plotted in Fig. 3 (b). The steady increase of $\text{Re } \hat{\sigma}$ with decreasing temperature shows that the entropy production process dominates the decrease of the soft-mode damping. As before, the sign change of $\text{Im } \hat{\sigma}$ for low temperatures can be clearly revealed. Due to the low temperatures regarded, $|\hat{\sigma}|$ shows a rapid increase for decreasing temperatures. In agreement with the absence of a theoretical ferroelectric transition at low temperatures, the soft mode frequency remains finite at low temperatures. As a result, the soft-mode peaks at $2\omega_0$ in $\mathcal{F}_\omega \langle u^2 \rangle_{\text{neq}}$ remain at higher frequencies, compared to SrTiO₃. Furthermore, the peaks occur fairly close to the maxima of $|\hat{\sigma}|$ making the entropion broadening less pronounced, in comparison to SrTiO₃.

CONCLUSION

We provide one of the first studies of ultrafast thermodynamic processes, by deriving the ultrafast entropy production due to transient phonons in materials excited by a THz laser pulse. Specifically, the soft modes of SrTiO₃ and KTaO₃ are evaluated by comparing our theory to experimental data and simulation results. The entropy production takes place on the picosecond timescale and can be deduced from the collective ionic displacement as observed, e.g., by time-resolved X-ray scattering. While entropy production and sample heating are well-known concepts in general, our work sheds light on the microscopic mechanism behind entropy production in driven quantum materials, using the framework of stochastic thermodynamics. While the maximal energy transfer from the laser to the sample is determined by the laser intensity, the production of entropy strongly increases with decreasing temperature. Furthermore, the temporal signature of this process is tightly bound to the soft mode frequency.

More generally, we envision ultrafast thermodynamics to provide characteristic signatures of complex systems, beyond phononic processes. We showed, in particular, that, in the presence of uncorrelated noise, entropy production depends on the materials' response function. As a consequence, Eq. (4) can be applied to other systems, e.g., magnons [9, 17, 71], considering the corresponding magnetic susceptibility.

Furthermore, our theory for the power spectrum of the displacement-displacement correlation exhibits spectral weight besides a sharp peak at twice the eigenfrequency of the soft mode. We have shown that this part of the power spectrum can be associated with spectral entropy production. The emergence of such a feature is closely related to the concept of entropions recently introduced for intrinsic non-equilibrium systems reaching a steady-state [68]. In contrast, here, the system is away from the steady state, and entropy production is generated by the transient force due to laser pulses.

ACKNOWLEDGEMENTS

We thank Jérémy Vachier for valuable insights and discussions. LC acknowledges support from the Alexander Von Humboldt foundation. HL acknowledges support by the Deutsche Forschungsgemeinschaft (DFG) through the SPP 2265 under the grant number LO 418/25-1. RMG acknowledges support from the Swedish Research Council (VR starting grant No. 2022-03350) and Chalmers University of Technology. Computational resources were provided by the Swedish National Infrastructure for Computing (SNIC) via the National Super-computer Centre (NSC).

APPENDIX

Spectral entropy production

By applying the time Fourier transform to the equation of motion for $u(t)$, Eq. (1) (see Fig. 4 for an example of its solution in real-time), we obtain the dynamics in the domain of frequency ω

$$(-\omega^2 + \omega_0^2 + i\omega\eta) \hat{u}(\omega) = \sqrt{2\eta k_B T} \hat{\xi}(\omega) + \hat{F}(\omega), \quad (9)$$

where the hat-symbol denotes the time-Fourier transform of a variable and $\hat{\xi}(\omega)$ is a Gaussian noise with zero average and $\langle \hat{\xi}(\omega) \hat{\xi}(\omega') \rangle = \delta(\omega + \omega')$. By defining the vector $v(t) = \dot{u}(t)$,

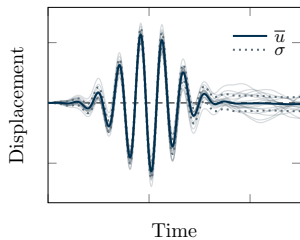


FIG. 4. Illustration of an ensemble of solutions of the equation of motion with uncorrelated noise for generic parameters. The blue solid line represents the mean solution, while dashed lines are single trajectories that illustrate the standard deviation.

so that $\hat{v}(\omega) = i\omega \hat{u}(\omega)$, Eq. (9) can be expressed as

$$i\omega \hat{u}(\omega) = \hat{v}(\omega) \quad (10)$$

$$(i\omega + \eta) \hat{v}(\omega) + \omega_0^2 \hat{u}(\omega) = \sqrt{2\eta k_B T} \hat{\xi}(\omega) + \hat{F}(\omega). \quad (11)$$

The path-probability of the phonon normal mode, $P[\{u\}|u_0]$, conditioned to the initial value u_0 , can be estimated by the probability distribution of the noise history $p[\{\xi\}|\xi_0]$, conditioned to the initial value ξ_0 . Here, curly brackets denote the time history from the initial to the final time. The Gaussian properties of the noise allows us to express $p[\{\xi\}|\xi_0]$ as [61]

$$\begin{aligned} p[\{\xi\}|\xi_0] &\sim \exp\left(-\frac{1}{2} \int dt \xi(t)^2\right) \\ &= \exp\left(-\frac{1}{2} \int dt \int \frac{d\omega}{2\pi} e^{-i\omega t} \int ds e^{i\omega s} \xi(s)^2\right) \\ &= \exp\left(-\frac{1}{2} \int dt \int \frac{d\omega}{2\pi} e^{-i\omega t} \int \frac{d\omega'}{2\pi} \hat{\xi}(\omega') \hat{\xi}(\omega - \omega')\right), \end{aligned} \quad (12)$$

where in the second and third equalities we have applied the properties of Fourier transforms. From here, we can switch to the probability of the trajectory for the phonon mode $\{u\}$ by handling the change of variables $\xi \rightarrow u$, i.e. by using the equation of motion in Fourier space

$$\hat{\xi}(\omega) = \frac{1}{\sqrt{2\eta k_B T}} \left[(i\omega + \eta) \hat{v}(\omega) + \omega_0^2 \hat{u}(\omega) - \hat{F}(\omega) \right]. \quad (13)$$

Such a change of variables should involve the determinant of the transformation. We ignore this term because it is irrelevant to the calculation of the entropy production since it provides only an even term under time-reversal transformation [61]. As a consequence, the following relation holds

$$P[\{u\}|u_0] \sim p[\{\xi\}|\xi_0]. \quad (14)$$

The path-probability of the backward trajectory of the phonon normal mode, $P_r[\{u\}|u_0]$, can be obtained by simply applying the time-reversal transformation (TRT) to the particle dynamics. By denoting time-reversed variables by a subscript r , the path-probability of the time-reversed noise history, $p_r[\{\xi\}|\xi_0]$, is still Gaussian and reads

$$\begin{aligned} p_r[\{\xi\}|\xi_0] &\sim \exp\left(-\frac{1}{2} \int dt \xi_r(t)^2\right) \\ &= \exp\left(-\frac{1}{2} \int dt \int \frac{d\omega}{2\pi} e^{-i\omega t} \int \frac{d\omega'}{2\pi} \hat{\xi}_r(\omega') \hat{\xi}_r(\omega - \omega')\right). \end{aligned} \quad (15)$$

To switch to $P_r[\{\xi\}|\xi_0]$, we first have to evaluate the backward dynamics, by simply applying the TRT to Eq. (1). By using $u_r = u$ and $v_r = -v$, we conclude that all the terms in Eq. (1) are invariant under TRT except for the friction force. Applying the Fourier transform to Eq. (1) and expressing the noise $\hat{\xi}_r(\omega)$ as a function of $u_r(\omega)$ and $v_r(\omega)$, we can recur to the change of variable $\xi_r \rightarrow u$ that allows us to use the following relation

$$\hat{\xi}_r(\omega) = \frac{1}{\sqrt{2\eta k_B T}} \left[(i\omega - \eta) \hat{v}(\omega) + \omega_0^2 \hat{u}(\omega) - \hat{F}(\omega) \right]. \quad (16)$$

By neglecting again the determinant of the change of variables, $P_r[\{u\}|u_0]$ reads

$$P_r[\{u\}|u_0] \sim p_r[\{\xi\}|\xi_0]. \quad (17)$$

To calculate the entropy production Σ , we use the definition (3), i.e. the log-ratio between the probabilities of forward and backward trajectories of the phonon normal mode,

$$\begin{aligned} (2T)\Sigma &= (2k_B T) \log \frac{p(\{u\}|u_0)}{p_r(\{u\}|u_0)} \\ &= \int dt \int \frac{d\omega}{2\pi} e^{-i\omega t} \int \frac{d\omega'}{2\pi} \times \\ &\quad \times \left(\langle \hat{v}(\omega') \hat{F}(\omega - \omega') \rangle + \langle \hat{v}(\omega - \omega') \hat{F}(\omega') \rangle \right). \end{aligned} \quad (18)$$

By comparing Eq. (18) with the definition

$$\Sigma = \int dt \dot{s}(t), \quad (19)$$

one can identify the entropy production rate, $\dot{s}(t)$, as

$$\begin{aligned} \dot{s}(t) &= \int \frac{d\omega}{2\pi} e^{-i\omega t} \int \frac{d\omega'}{2\pi} \frac{1}{2T} \times \\ &\quad \times \left(\langle \hat{v}(\omega') \hat{F}(\omega - \omega') \rangle + \langle \hat{v}(\omega - \omega') \hat{F}(\omega') \rangle \right). \end{aligned} \quad (20)$$

Applying the Fourier transform, we introduce the spectral entropy production rate, $\hat{s}(\omega)$, as

$$\hat{s}(\omega) = \int \frac{d\omega'}{2\pi} e^{-i\omega t} \hat{s}(\omega) \quad (21)$$

and, by comparison with Eq. (20), we obtain

$$\hat{s}(\omega) = \int \frac{d\omega'}{2\pi} \frac{1}{2k_B T} \left(\langle \hat{v}(\omega') \hat{F}(\omega - \omega') \rangle + \langle \hat{v}(\omega - \omega') \hat{F}(\omega') \rangle \right). \quad (22)$$

We remark that expressions (18) and (22) do not depend on the choice of the force in the dynamics of $\hat{u}(\omega)$. As a result, they are unchanged by adding a non-linear force, e.g., due to phonon-phonon coupling to Equation (9).

Entropy spectral density

The formal solution of the equation of motion (1) in Fourier space is given by

$$\hat{u}(\omega) = \frac{\sqrt{2\eta k_B T} \hat{\xi}(\omega) + \hat{F}(\omega)}{\omega_0^2 - \omega^2 + i\omega\eta} = \chi(\omega) \hat{A}(\omega). \quad (23)$$

Here, $\chi(\omega)$ is the (linear) susceptibility

$$\chi(\omega) = \frac{1}{\omega_0^2 - \omega^2 + i\omega\eta}, \quad (24)$$

and $\hat{A}(\omega) = \sqrt{2\eta k_B T} \hat{\xi}(\omega) + \hat{F}(\omega)$. By using that $\hat{v}(\omega) = i\omega \hat{u}(\omega)$ and $\langle \hat{\xi}(\omega) \rangle$, the spectral entropy production, $\hat{s}(\omega)$, can be expressed as

$$\hat{s}(\omega) = \frac{i}{T} \int \frac{d\omega'}{2\pi} k \hat{F}(\omega - \omega') \chi(\omega') F(\omega'). \quad (25)$$

By introducing the entropy spectral density, $\hat{S}_r(\omega, \omega')$, as

$$\hat{s}(\omega) = \int \frac{d\omega'}{2\pi} \hat{S}_r(\omega, \omega'), \quad (26)$$

we can immediately identify

$$\hat{S}_r(\omega, \omega') = \frac{(i\omega')}{T} \hat{F}(\omega - \omega') \chi(\omega') F(\omega'). \quad (27)$$

Equation (27) coincides with formula (5) of the main text. Non-linear force terms do not allow the system to have a formal solution in terms of $\chi(\omega)$. Thus, formula (27) holds only in the linear case.

Dynamical correlation of the normal phonon mode

By using Eq. (23) the Fourier transform of the dynamical correlation, $\mathcal{F}\langle u^2(t) \rangle$, is given by

$$\begin{aligned} \mathcal{F}\langle u^2(t) \rangle &= \int \frac{d\omega'}{2\pi} \langle \hat{u}(\omega') \hat{u}(\omega - \omega') \rangle \\ &= \int \frac{d\omega'}{2\pi} \langle \hat{A}(\omega') \hat{A}(\omega - \omega') \rangle \hat{\chi}(\omega') \hat{\chi}(\omega - \omega'). \end{aligned} \quad (28)$$

First, we applied the convolution theorem and, second, we used Eq. (23). Using the definition of $\hat{A}(\omega)$, $\mathcal{F}\langle u^2(t) \rangle$ can be decomposed into two terms,

$$\mathcal{F}\langle u^2(t) \rangle = \mathcal{F}\langle u^2(t) \rangle_{eq} + \mathcal{F}\langle u^2(t) \rangle_{neq}. \quad (29)$$

The first term, $\mathcal{F}\langle u^2(t) \rangle_{eq}$, in the right-hand side of Eq. (28), has an equilibrium origin: it arises from the Brownian noise and is given by the convolution of the susceptibility with itself. For uncorrelated noise, we have $\langle \hat{\xi}(\omega') \hat{\xi}(\omega - \omega') \rangle = \delta(\omega)$, and this term reads

$$\begin{aligned} \mathcal{F}\langle u^2(t) \rangle_{eq} &= 2\eta k_B T \int \frac{d\omega'}{2\pi} \langle \hat{\xi}(\omega') \hat{\xi}(\omega - \omega') \rangle \hat{\chi}(\omega') \hat{\chi}(\omega - \omega') \\ &= 2\eta k_B T \delta(\omega) \int \frac{d\omega'}{2\pi} \hat{\chi}(\omega') \hat{\chi}(-\omega'). \end{aligned} \quad (30)$$

As an equilibrium term, $\mathcal{F}\langle u^2(t) \rangle_{eq}$ gives a DC contribution ($\omega = 0$) to the dynamical correlation and does not prevent the system from reaching a steady state.

In contrast, the second term $\mathcal{F}\langle u^2(t) \rangle_{neq}$ in the right-hand side of Eq. (28) has a non-equilibrium origin. It disappears when the non-equilibrium force vanishes and is given by

$$\mathcal{F}\langle u^2(t) \rangle_{neq} = \int \frac{d\omega'}{2\pi} \hat{F}(\omega') \hat{F}(\omega - \omega') \hat{\chi}(\omega') \hat{\chi}(\omega - \omega'). \quad (31)$$

This term can be linked to the entropy spectral density $S_r(\omega, \omega')$, defined in Eq. (27). As a result, Eq. (31), can be written as follows,

$$\mathcal{F}\langle u^2(t) \rangle_{neq} = T \int \frac{d\omega'}{2\pi} \frac{\hat{\chi}(\omega - \omega')}{(i\omega')} \hat{S}_r(\omega, \omega'), \quad (32)$$

which corresponds to Eq. (8) of the main text.

Temperature dependence of the soft mode

The soft mode frequency and the damping or line width are strongly temperature dependent. We model the temperature dependence from data taken from Vogt [64] and fitting to a second-order polynomial,

$$x(T) = a_0 + a_1 T + a_2 T^2. \quad (33)$$

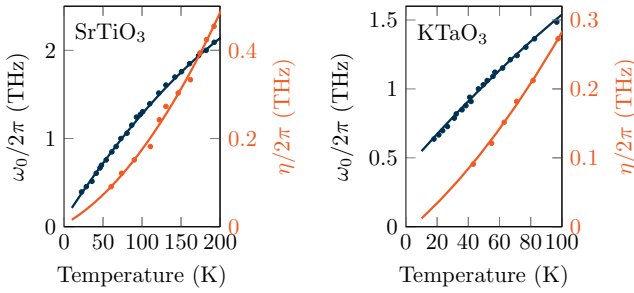


FIG. 5. Temperature dependence of the soft mode frequency (blue) and damping (orange) for SrTiO₃ and KTaO₃. Dots correspond to experimental data taken from Vogt [64]. Solid lines show the quadratic fit for comparison.

	a_0 (THz)	a_1 (THz/K)	a_2 (THz/K ²)
SrTiO ₃	ω_0	0.078	-17×10^{-6}
	η	0.005	7×10^{-6}
KTaO ₃	ω_0	0.42	-18×10^{-6}
	η	-0.008	10×10^{-6}

TABLE I. Fitting parameters for the temperature dependence of the soft mode frequency ω_0 and the damping η for SrTiO₃ and KTaO₃.

Here, $x = \omega_0, \eta$ is either the soft mode frequency ω_0 or the damping η . In the past, other parametrizations of the soft mode have been proposed, e.g., the four-parameter model by Barrett [72]. However, for our purpose, a fit according to Eq. (33) provides a reasonable accuracy within the discussed temperature range. The fitting parameters are given in Tab. I, while a comparison of the quadratic fit with experimental data is reported in Fig. 5 for SrTiO₃ and KTaO₃ materials, showing good agreement both for the soft mode frequency and damping.

* lorenzo.caprini@gssi.it

† matthias.geilhufe@chalmers.se

- [1] P. Nazé, Convex entropy production for fast and weak drivings, arXiv:2210.11975 (2022).
- [2] S. R. De Groot and P. Mazur, *Non-equilibrium thermodynamics* (Courier Corporation, 2013).
- [3] C. E. Shannon, A mathematical theory of communication, The Bell System Technical Journal **27**, 379 (1948).
- [4] U. Seifert, Stochastic thermodynamics, fluctuation theorems and molecular machines, Reports on Progress in Physics **75**, 126001 (2012).
- [5] C. Jarzynski, Equalities and inequalities: Irreversibility and the second law of thermodynamics at the nanoscale, Annual Review of Condensed Matter Physics **2**, 329 (2011).
- [6] J. O'Byrne, Y. Kafri, J. Tailleur, and F. van Wijland, Time irreversibility in active matter, from micro to macro, Nature Reviews Physics **4**, 167 (2022).
- [7] L. Peliti and S. Pigolotti, *Stochastic Thermodynamics: An Introduction* (Princeton University Press, 2021).
- [8] A. N. Koya, M. Romanelli, J. Kuttruff, N. Henriksson, A. Stefancu, G. Grinblat, A. De Andres, F. Schmur, M. Vanzan, M. Marsili, *et al.*, Advances in ultrafast plasmonics, arXiv:2211.08241 (2022).
- [9] P. Scheid, Q. Remy, S. Lebègue, G. Malinowski, and S. Mangin, Light induced ultrafast magnetization dynamics in metallic compounds, Journal of Magnetism and Magnetic Materials **560**, 169596 (2022).
- [10] E. Cinquanta, E. A. A. Pogna, L. Gatto, S. Stagira, and C. Vozzi, Charge carrier dynamics in 2D materials probed by ultrafast THz spectroscopy, Advances in Physics: X **8**, 2120416 (2022).
- [11] M. Guan, D. Chen, S. Hu, H. Zhao, P. You, and S. Meng, Theoretical insights into ultrafast dynamics in quantum materials, Ultrafast Science **2022** (2022).
- [12] Y. Zhang, J. Dai, X. Zhong, D. Zhang, G. Zhong, and J. Li, Probing ultrafast dynamics of ferroelectrics by time-resolved pump-probe spectroscopy, Advanced Science **8**, 2102488 (2021).
- [13] C. Jin, E. Y. Ma, O. Karni, E. C. Regan, F. Wang, and T. F. Heinz, Ultrafast dynamics in van der Waals heterostructures, Nature Nanotechnology **13**, 994 (2018).
- [14] H. Yang, S. Sun, M. Zhang, Z. Li, Z. Li, P. Xu, H. Tian, and J. Li, Ultrafast electron microscopy in material science, Chinese Physics B **27**, 070703 (2018).
- [15] Y. Tian, F. Yang, C. Guo, and Y. Jiang, Recent advances in ultrafast time-resolved scanning tunneling microscopy, Surface Review and Letters **25**, 1841003 (2018).
- [16] J. Zhu, X. Wu, D. M. Lattery, W. Zheng, and X. Wang, The ultrafast laser pump-probe technique for thermal characterization of materials with micro/nanostructures, Nanoscale and Microscale Thermophysical Engineering **21**, 177 (2017).
- [17] A. M. Kalashnikova, A. V. Kimel, and R. V. Pisarev, Ultrafast opto-magnetism, Physics-Uspekhi **58**, 969 (2015).
- [18] J.-Y. Bigot and M. Vomir, Ultrafast magnetization dynamics of nanostructures, Annalen der Physik **525**, 2 (2013).
- [19] S. Yoshida, Y. Terada, M. Yokota, O. Takeuchi, H. Oigawa, and H. Shigekawa, Optical pump-probe scanning tunneling microscopy for probing ultrafast dynamics on the nanoscale, The European Physical Journal Special Topics **222**, 1161 (2013).
- [20] M. Chergui and A. H. Zewail, Electron and X-ray methods of ultrafast structural dynamics: Advances and applications, ChemPhysChem **10**, 28 (2009).
- [21] M. Basini, M. Udina, M. Pancaldi, V. Unikandanunni, S. Bonetti, *et al.*, Terahertz ionic kerr effect, arXiv:2210.14053 (2022).
- [22] M. Basini, M. Pancaldi, B. Wehinger, M. Udina, T. Tadano, M. Hoffmann, A. Balatsky, and S. Bonetti, Terahertz electric-field driven dynamical multiferroicity in SrTiO₃, arXiv:2210.01690 (2022).
- [23] M. Kozina, M. Fechner, P. Marsik, T. van Driel, J. M. Glowia, C. Bernhard, M. Radovic, D. Zhu, S. Bonetti, U. Staub, *et al.*, Terahertz-driven phonon upconversion in SrTiO₃, Nature Physics **15**, 387 (2019).
- [24] A. von Hoegen, R. Mankowsky, M. Fechner, M. Först, and A. Cavalleri, Probing the interatomic potential of solids with strong-field nonlinear phononics, Nature **555**, 79 (2018).
- [25] A. Cartella, T. F. Nova, M. Fechner, R. Merlin, and A. Cavalleri, Parametric amplification of optical phonons, Proceedings of the National Academy of Sci-

- ences **115**, 12148 (2018).
- [26] R. Li, K. Sundqvist, J. Chen, H. Elsayed-Ali, J. Zhang, and P. M. Rentzepis, Transient lattice deformations of crystals studied by means of ultrafast time-resolved X-ray and electron diffraction, *Structural Dynamics* **5**, 044501 (2018).
- [27] R. Mankowsky, M. Fechner, M. Först, A. von Hoegen, J. Porras, T. Loew, G. Dakovski, M. Seaberg, S. Möller, G. Coslovich, *et al.*, Optically induced lattice deformations, electronic structure changes, and enhanced superconductivity in $\text{YBa}_2\text{Cu}_3\text{O}_{6.48}$, *Structural Dynamics* **4**, 044007 (2017).
- [28] M. Kozina, T. van Driel, M. Chollet, T. Sato, J. Glownia, S. Wandel, M. Radovic, U. Staub, and M. Hoffmann, Ultrafast X-ray diffraction probe of terahertz field-driven soft mode dynamics in SrTiO_3 , *Structural Dynamics* **4**, 054301 (2017).
- [29] L. Rettig, S. O. Mariager, A. Ferrer, S. Grübel, J. A. Johnson, J. Rittmann, T. Wolf, S. L. Johnson, G. Ingold, P. Beaud, and U. Staub, Ultrafast structural dynamics of the Fe-pnictide parent compound BaFe_2As_2 , *Physical Review Letters* **114**, 067402 (2015).
- [30] R. Mankowsky, A. Subedi, M. Först, S. O. Mariager, M. Chollet, H. Lemke, J. S. Robinson, J. M. Glownia, M. P. Minitti, A. Frano, *et al.*, Nonlinear lattice dynamics as a basis for enhanced superconductivity in $\text{YBa}_2\text{Cu}_3\text{O}_{6.5}$, *Nature* **516**, 71 (2014).
- [31] L. X. Yang, G. Rohde, T. Rohwer, A. Stange, K. Hanff, C. Sohrt, L. Rettig, R. Cortés, F. Chen, D. L. Feng, T. Wolf, B. Kamble, I. Eremin, T. Popmintchev, M. M. Murnane, H. C. Kapteyn, L. Kipp, J. Fink, M. Bauer, U. Bovensiepen, and K. Rossnagel, Ultrafast modulation of the chemical potential in bafe_2as_2 by coherent phonons, *Physical Review Letters* **112**, 207001 (2014).
- [32] M. Först, R. Mankowsky, H. Bromberger, D. M. Fritz, H. Lemke, D. Zhu, M. Chollet, Y. Tomioka, Y. Tokura, R. Merlin, *et al.*, Displacive lattice excitation through nonlinear phononics viewed by femtosecond X-ray diffraction, *Solid State Communications* **169**, 24 (2013).
- [33] P. Salén, M. Basini, S. Bonetti, J. Hebling, M. Krasilnikov, A. Y. Nikitin, G. Shamuilov, Z. Tibai, V. Zhaunerchyk, and V. Goryashko, Matter manipulation with extreme terahertz light: Progress in the enabling thz technology, *Physics Reports* **836**, 1 (2019).
- [34] T. Kampfrath, K. Tanaka, and K. A. Nelson, Resonant and nonresonant control over matter and light by intense terahertz transients, *Nature Photonics* **7**, 680 (2013).
- [35] R. Schoenlein, T. Elsaesser, K. Holldack, Z. Huang, H. Kapteyn, M. Murnane, and M. Woerner, Recent advances in ultrafast X-ray sources, *Philosophical Transactions of the Royal Society A* **377**, 20180384 (2019).
- [36] M. Buzzi, M. Först, and A. Cavalleri, Measuring nonequilibrium dynamics in complex solids with ultrashort x-ray pulses, *Philosophical Transactions of the Royal Society A* **377**, 20170478 (2019).
- [37] H.-S. Kang, C.-K. Min, H. Heo, C. Kim, H. Yang, G. Kim, I. Nam, S. Y. Baek, H.-J. Choi, G. Mun, *et al.*, Hard X-ray free-electron laser with femtosecond-scale timing jitter, *Nature Photonics* **11**, 708 (2017).
- [38] C. J. Milne, T. Schietinger, M. Aiba, A. Alarcon, J. Alex, A. Anghel, V. Arsov, C. Beard, P. Beaud, S. Bettoni, *et al.*, SwissFEL: the Swiss X-ray free electron laser, *Applied Sciences* **7**, 720 (2017).
- [39] C. Bostedt, S. Boutet, D. M. Fritz, Z. Huang, H. J. Lee, H. T. Lemke, A. Robert, W. F. Schlotter, J. J. Turner, and G. J. Williams, Linac coherent light source: The first five years, *Reviews of Modern Physics* **88**, 015007 (2016).
- [40] E. Allaria, L. Badano, S. Bassanese, F. Capotondi, D. Castronovo, P. Cinquegrana, M. Danailov, G. D’auria, A. Demidovich, R. De Monte, *et al.*, The FERMI free-electron lasers, *Journal of Synchrotron Radiation* **22**, 485 (2015).
- [41] M. Yabashi, H. Tanaka, and T. Ishikawa, Overview of the SACLA facility, *Journal of Synchrotron Radiation* **22**, 477 (2015).
- [42] S. Ackermann, A. Azima, S. Bajt, J. Bödewadt, F. Curbis, H. Dachraoui, H. Delsim-Hashemi, M. Drescher, S. Düsterer, B. Faatz, *et al.*, Generation of coherent 19-and 38-nm radiation at a free-electron laser directly seeded at 38 nm, *Physical Review Letters* **111**, 114801 (2013).
- [43] E. Allaria, D. Castronovo, P. Cinquegrana, P. Craievich, M. Dal Forno, M. Danailov, G. D’Auria, A. Demidovich, G. De Ninno, S. Di Mitri, *et al.*, Two-stage seeded soft-X-ray free-electron laser, *Nature Photonics* **7**, 913 (2013).
- [44] T. Ishikawa, H. Aoyagi, T. Asaka, Y. Asano, N. Azumi, T. Bizen, H. Ego, K. Fukami, T. Fukui, Y. Furukawa, *et al.*, A compact X-ray free-electron laser emitting in the sub-ångström region, *Nature Photonics* **6**, 540 (2012).
- [45] P. Emma, R. Akre, J. Arthur, R. Bionta, C. Bostedt, J. Bozek, A. Brachmann, P. Bucksbaum, R. Coffee, F.-J. Decker, *et al.*, First lasing and operation of an ångström-wavelength free-electron laser, *Nature Photonics* **4**, 641 (2010).
- [46] W. a. Ackermann, G. Asova, V. Ayvazyan, A. Azima, N. Baboi, J. Bähr, V. Balandin, B. Beutner, A. Brandt, A. Bolzmann, *et al.*, Operation of a free-electron laser from the extreme ultraviolet to the water window, *Nature Photonics* **1**, 336 (2007).
- [47] J. M. Madey, Stimulated emission of bremsstrahlung in a periodic magnetic field, *Journal of Applied Physics* **42**, 1906 (1971).
- [48] R. M. Geilhufe and W. Hergert, Electron magnetic moment of transient chiral phonons in KTaO_3 , arXiv:2208.05746 (2022).
- [49] R. M. Geilhufe, V. Juričić, S. Bonetti, J.-X. Zhu, and A. V. Balatsky, Dynamically induced magnetism in KTaO_3 , *Physical Review Research* **3**, L022011 (2021).
- [50] D. M. Juraschek, T. Neuman, and P. Narang, Giant effective magnetic fields from optically driven chiral phonons in $4f$ paramagnets, *Physical Review Research* **4**, 013129 (2022).
- [51] D. M. Juraschek and N. A. Spaldin, Orbital magnetic moments of phonons, *Physical Review Materials* **3**, 064405 (2019).
- [52] D. M. Juraschek, M. Fechner, and N. A. Spaldin, Ultrafast structure switching through nonlinear phononics, *Physical Review Letters* **118**, 054101 (2017).
- [53] D. M. Juraschek, M. Fechner, A. V. Balatsky, and N. A. Spaldin, Dynamical multiferroicity, *Physical Review Materials* **1**, 014401 (2017).
- [54] M. Fechner and N. A. Spaldin, Effects of intense optical phonon pumping on the structure and electronic properties of yttrium barium copper oxide, *Physical Review B* **94**, 134307 (2016).
- [55] R. Mankowsky, A. von Hoegen, M. Först, and A. Cavalleri, Ultrafast reversal of the ferroelectric polarization,

- Physical Review Letters **118**, 197601 (2017).
- [56] A. Subedi, A. Cavalleri, and A. Georges, Theory of nonlinear phononics for coherent light control of solids, *Physical Review B* **89**, 220301 (2014).
- [57] X. Gonze and C. Lee, Dynamical matrices, Born effective charges, dielectric permittivity tensors, and interatomic force constants from density-functional perturbation theory, *Physical Review B* **55**, 10355 (1997).
- [58] M. Henstridge, M. Först, E. Rowe, M. Fechner, and A. Cavalleri, Nonlocal nonlinear phononics, *Nature Physics* **18**, 457 (2022).
- [59] C. Tietz, S. Schuler, T. Speck, U. Seifert, and J. Wrachtrup, Measurement of stochastic entropy production, *Physical Review Letters* **97**, 050602 (2006).
- [60] L. Dabelow, S. Bo, and R. Eichhorn, Irreversibility in active matter systems: Fluctuation theorem and mutual information, *Physical Review X* **9**, 021009 (2019).
- [61] L. Caprini, U. M. B. Marconi, A. Puglisi, and A. Vulpiani, The entropy production of Ornstein–Uhlenbeck active particles: a path integral method for correlations, *Journal of Statistical Mechanics: Theory and Experiment* **2019**, 053203 (2019).
- [62] D. M. Juraschek and N. A. Spaldin, Orbital magnetic moments of phonons, *Physical Review Materials* **3**, 064405 (2019).
- [63] R. M. Geilhufe, V. Juričić, S. Bonetti, J.-X. Zhu, and A. V. Balatsky, Dynamically induced magnetism in KTaO_3 , *Physical Review Research* **3**, L022011 (2021).
- [64] H. Vogt, Refined treatment of the model of linearly coupled anharmonic oscillators and its application to the temperature dependence of the zone-center soft-mode frequencies of KTaO_3 and SrTiO_3 , *Physical Review B* **51**, 8046 (1995).
- [65] D. Bäuerle, D. Wagner, M. Wöhlecke, B. Dorner, and H. Kraxenberger, Soft modes in semiconducting SrTiO_3 : II. the ferroelectric mode, *Zeitschrift für Physik B Condensed Matter* **38**, 335 (1980).
- [66] R. Loetzsch, A. Lübcke, I. Uschmann, E. Förster, V. Große, M. Thuerk, T. Koettig, F. Schmidl, and P. Seidel, The cubic to tetragonal phase transition in SrTiO_3 single crystals near its surface under internal and external strains, *Applied Physics Letters* **96**, 071901 (2010).
- [67] K. A. Müller and H. Burkard, SrTiO_3 : An intrinsic quantum paraelectric below 4 K, *Physical Review B* **19**, 3593 (1979).
- [68] L. Caprini, U. M. B. Marconi, A. Puglisi, and H. Löwen, Entropions as collective excitations in active solids, *arXiv:2207.02369* (2022).
- [69] M. E. Lines and A. M. Glass, *Principles and applications of ferroelectrics and related materials* (Oxford university press, 2001).
- [70] S. Rowley, L. Spalek, R. Smith, M. Dean, M. Itoh, J. Scott, G. Lonzarich, and S. Saxena, Ferroelectric quantum criticality, *Nature Physics* **10**, 367 (2014).
- [71] A. El-Ghazaly, J. Gorchon, R. B. Wilson, A. Pattabi, and J. Bokor, Progress towards ultrafast spintronics applications, *Journal of Magnetism and Magnetic Materials* **502**, 166478 (2020).
- [72] J. H. Barrett, Dielectric constant in perovskite type crystals, *Physical Review* **86**, 118 (1952).